Viscosity and real-space molecular motion of water: Observation with inelastic x-ray scattering

Yuya Shinohara,[1] Wojciech Dmowski,[1] Takuya Iwashita,[2] Bin Wu,[3] Daisuke Ishikawa,[4,5] Alfred Q. R. Baron,[4] and Takeshi Egami[1,3,6]

[1]*Shull-Wollan Center, University of Tennessee and Oak Ridge National Laboratory, Oak Ridge, Tennessee, 37831, USA and Department of Materials Science and Engineering, University of Tennessee, Knoxville, Tennessee, 37996, USA*

[2]*Department of Integrated Science and Technology, Oita University, Dannoharu, Oita 870-1192, Japan*

[3]*Oak Ridge National Laboratory, Oak Ridge, Tennessee, 37831, USA*

[4]*Materials Dynamics Laboratory, RIKEN SPring-8 Center, RIKEN, Sayo, Hyogo 679-5148, Japan*

[5]*Research and Utilization Divition, Japan Synchrotron Radiation Research Institute (JASRI), Sayo, Hyogo 679-5198, Japan*

[6]*Department of Physics and Astronomy, University of Tennessee, Knoxville, Tennessee 37996, USA*

(Received 11 January 2018; published 10 August 2018)

Even though viscosity is one of the fundamental properties of liquids, its microscopic origin is not fully understood. We determined the spatial and temporal correlation of molecular motions of water near room temperature and its temperature variation on a picosecond timescale and a subnanometer spatial scale, through high-resolution inelastic x-ray scattering measurement. The results, expressed in terms of the time-dependent pair correlation function called the Van Hove function, show that the timescale of the decay of the molecular correlation is directly related to the Maxwell relaxation time near room temperature, which is proportional to viscosity. This conclusion validates our earlier finding that the topological changes in atomic or molecular connectivity are the origin of viscosity in liquids.

DOI: 10.1103/PhysRevE.98.022604

I. INTRODUCTION

Water is a material that is fundamental to life. Nevertheless, its properties, structure, and dynamics at the molecular level are still under intense debate [1–6]. Water exhibits many anomalous features, such as the unusual temperature variations in density, isobaric heat capacity, and isothermal compressibility [7]. It is suspected that the hydrogen bond in water, which is highly quantum mechanical, is primarily responsible for these anomalies [8]. To understand the physical origin of these properties, the structure and dynamics of water molecules have been extensively studied using x-ray and neutron scattering [9–21] and optical spectroscopy [22–27] as well as computer simulation [28–33]. However, the structure has been characterized mainly by a snapshot atomic correlation function determined by diffraction measurement which lacks dynamical information, whereas the dynamics has been studied primarily by spectroscopic analysis which does not provide information on spatial correlation. Thus, the precise details of molecular motions of water in real space and real time are poorly understood despite a vast amount of study.

Recently, we reported the observation of the spatial and temporal correlation of water molecules through the Van Hove function [34] determined by inelastic x-ray scattering (IXS) measurement [35]. The molecular Van Hove function is defined as

$$G(R,t) = \frac{1}{4\pi\rho N R^2} \sum_{i,j} \delta[R - |r_i(0) - r_j(t)|], \qquad (1)$$

where ρ is the average number density of molecules, N is the number of molecules in the system, and $r_i(t)$ is the position of the ith molecule at time t. The Van Hove function describes the probability for a molecule at the origin $R = 0$ at time $t = 0$ finding another molecule at distance R at time t. $G(R, t)$ can be obtained by the double Fourier transformation of the dynamic structure factor, $S(Q, E)$, over momentum transfer Q and energy transfer E [34]. Although many measurements of $S(Q, E)$ have already been carried out for the study of dynamics of liquid water [15,36,37], these studies focused principally on phonons. Consequently, $S(Q, E)$ was measured only at relatively low $Q(<2\,\text{Å}^{-1})$ where the phonon dispersion is clearly seen, and the high-Q range, where quasielastic scattering dominates, was never explored. However, in order to determine the Van Hove function, $S(Q, E)$ has to be measured over wide ranges of E and Q to minimize termination errors, just as the determination of the snapshot pair distribution function (PDF) of water requires the scattering data of $S(Q)$ over a wide range of Q [11]. Owing to the recent progress in x-ray beamlines and instrumentation [38,39], it is now possible to conduct IXS measurements with high resolution in E and Q over wide E and Q ranges [40,41] to allow accurate calculation of $G(R, t)$ [35]. The Van Hove function of liquid metal measured with inelastic neutron scattering was also recently reported [42]. Here we report the temperature dependence of the Van Hove function of water near room temperature obtained by high-resolution IXS measurement. Because an x ray is scattered mainly by oxygen atoms, the x ray $S(Q, E)$ is dominated by the oxygen-oxygen, thus intermolecular, correlations. By combining with molecular dynamics simulation, we obtained the detailed picture of the local motion of water molecules. The results present the molecular-level views on the origin of viscosity in water.

II. EXPERIMENTAL METHODS

A. Inelastic x-ray scattering

Inelastic x-ray scattering (IXS) measurements of water under ambient conditions were conducted at RIKEN Quantum NanoDynamics Beamline (BL43LXU) [43], SPring-8 (Hyogo, Japan). The sample was high-purity water and was kept at 285, 295, 310, and 318 K. The energy of the incident x rays was 21.747 keV and the scattered x rays were detected by an array of 4 × 6 backscattering Si analyzers at the end of the 10-m horizontal arm [41]. The energy resolution was 1.4–1.9 meV for each analyzer, as was estimated by the measurement of poly(methyl methacrylate), 2.0 mm in thickness, and the Q resolution was 0.4–1 Å^{-1}. Liquid water at the controlled temperature was placed between two single crystal diamond windows ($4 \times 4 \times 0.3\,\text{mm}^3$). The sample thickness was 3 mm. The measurement was made by scanning incident energy at a fixed scattering angle, and data were collected over a wide Q-E range ($0.94\,\text{Å}^{-1} < Q < 10.1\,\text{Å}^{-1}$, $-10\,\text{meV} < E < 100\,\text{meV}$).

B. Calculation of Van Hove function

The measured IXS data, $I_{\text{raw}}(Q, E)$, were reduced to the Van Hove function, $G(R, t)$, following the procedures discussed in the previous report [35]. Phonon contributions from the diamond windows were removed, and the scattering spectrum with large negative energy transfer down to −100 meV was constructed using the principle of detailed balance, $I_{\text{raw}}(Q, -E) = I_{\text{raw}}(Q, E)e^{-E/k_BT}$. After confirming that the profiles summed over the energy, $\int I_{\text{raw}}(Q, E)\text{d}E$, were proportional to the reported x-ray diffraction profiles measured with high-energy x rays, we normalized them to the absolute scattering intensity, by $I(Q, E) = I_X(Q)\,\frac{I_{\text{raw}}(Q,E)}{\int I_{\text{raw}}(Q,E)\text{d}E}$, where $I_X(Q)$ is the accurate x-ray diffraction data of water using high-energy x rays [44]. In this process, the detector efficiency and the absorption factor were also corrected. Then the dynamic structure function was calculated by $S(Q, E) = I(Q, E)/\langle f(Q, E)\rangle^2$, where $\langle f(Q, E)\rangle$ is the azimuthally averaged molecular form factor of water [45]. The intermediate scattering function, $F(Q, t)$, is given by the Fourier transform of $S(Q, E)$ over energy ($-100\,\text{meV} < E < 100\,\text{meV}$):

$$F(Q, t) = \int S(Q, E)e^{i\omega t}d\omega, \tag{2}$$

where $E = \hbar\omega$. The Van Hove function is given by the Fourier transform of $F(Q, t)$ in Q space:

$$G(R, t) - 1 = \frac{1}{2\pi^2\rho r}\int F(Q, t)\sin(Qr)QdQ, \tag{3}$$

where the integration over Q was done between 0.94 and 25 Å^{-1} for the IXS data. The measured Q range is limited to $Q < 10\,\text{Å}^{-1}$, and $F(Q = 10\,\text{Å}^{-1}, t < 0.1\,\text{ps})$ is not small enough so that the calculation of the Van Hove function is not free from termination errors accompanied by the Fourier transform in the limited Q space. To minimize the termination error we extrapolated $F(Q, t = 0)$ up to $Q = 25\,\text{Å}^{-1}$ using the reported value of scattering intensity [44], divided by the form factor of the water molecule. After that, the profiles of $F(Q, t \neq 0)$ up to $Q = 25\,\text{Å}^{-1}$ were extrapolated using $F(Q, t = 0)\exp[-w(t)Q^2]$ as demonstrated in the previous studies [35,46], because $F(Q, t)$ in the high-Q range is dominated by the self-correlation due to diffusion, the behavior of which is well understood. Furthermore, the Blackman-Harris window was used to reduce the termination errors of $G(R, t)$ at a short time ($t < 0.1$ ps).

C. Molecular dynamics calculation

Classical molecular dynamics (MD) simulations using the extended simple point charge (SPC/E) model were conducted to make a comparison with the experimental data. MD calculations were run by using LAMMPS [47,48]. Simulations were done in a cubic box with periodic boundary conditions. The temperature was fixed at 263, 278, 285, 295, 310, 318, and 324 K, and the pressure was set to 1 atm under the *NTP* ensemble. The number of molecules N was 10648. The Van Hove function was directly calculated using the trajectory of water molecules in real space and real time.

III. RESULTS

A. Van Hove function from IXS and MD simulation

Figure 1 shows the Van Hove function, $G(R, t)$, of water at various temperatures obtained from IXS. Both one-dimensional profiles and two-dimensional plots are shown to illustrate the real-time dynamics of water molecules in real space. At $t = 0$, the Van Hove function was in good agreement with the known snapshot pair distribution function obtained by x-ray diffraction, except for the small ripples below 2 Å due to the termination error caused by the limited ranges of Q and E in the IXS experiment. The peak (valley) positions and their heights (depths) evolve with time, representing the temporal changes in the positional correlations of water molecules in real space.

The Van Hove function consists of two parts: a self part which represents self-motions of molecules and a distinct part which represents mutual motions of pairs of different water molecules. In this measurement, the self part of the Van Hove function is mainly observed at $R < 1.5$ Å as the sharp peak around $R = 0$, while the distinct part is observed at larger R. Characteristic energies for intramolecular motion such as OH stretching (420 meV) and OH bend vibration (200 meV) are out of the measured energy range ($E < 100$ meV), so that such intramolecular motions are averaged out and not taken into account in the measured dynamics. The peak of the self part around $R = 0$ broadens and decays in intensity with time [Figs. 1(a)–1(d)], showing the self-diffusing behavior of water molecules. As the temperature of the water increases, the decay rates become fast, indicating the intensified self-motion as expected.

The distinct part of the Van Hove function exhibits three peaks in this R range and its time evolution displays behaviors similar to those reported in the previous study [35] [Figs. 1(e)–1(h)]; the first neighbor peak (R_1) around 2.8 Å at $t = 0$ moves away to larger distances and the second neighbor peak (R_2) around 4.5 Å at $t = 0$ moves inward to shorter distances [Fig. 2 (left)], whereas the position of the third peak remains largely unchanged. The first peak entirely decays after $t = 0.9$–1.3 ps, depending on the sample temperature. At higher temperatures (310 and 318 K), the position of the second

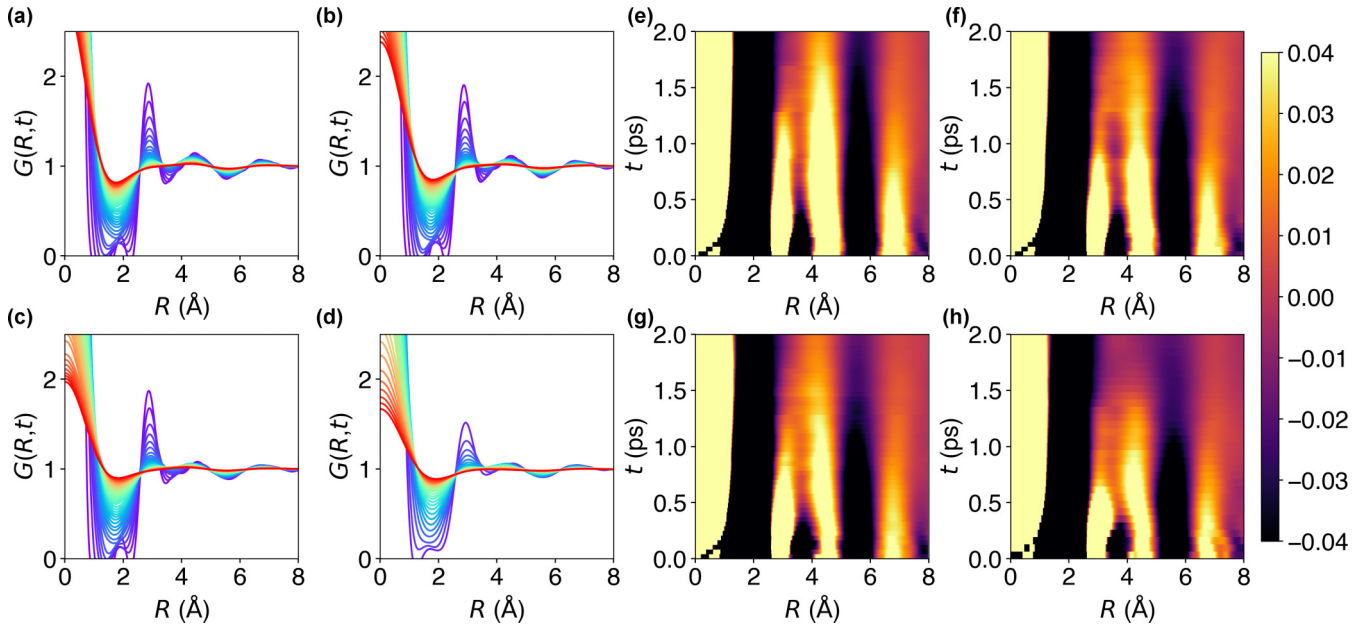

FIG. 1. Van Hove function of water at ambient temperatures obtained from IXS results. (a)–(d) One-dimensional profiles at 0.12 ps $<$ t $<$ 2 ps. The arrows indicate the direction of temporal evolution. (e)–(h) Intensity map of $G(R, t) - 1$. Note that a narrow range is used to highlight small changes in the second and third peaks. Temperature of the water was 285 K (a),(e), 295 K (b),(f), 310 K (c),(g), and 318 K (d),(h).

maximum shifts rather sharply up to $t = 0.6$ ps, followed by a slower change around 4.25 Å. The shifts in the positions of the first two maxima are markedly different from those of metallic liquids, where the peak positions of the Van Hove function are mostly independent of time [35,42,46]. This indicates the presence of dynamic coupling of the first and second neighbors in water, most likely related to the presence of a hydrogen bond, which will be discussed in a later section.

Qualitatively similar results were obtained by the MD simulation using the SPC/E model (Fig. 3). The position of the maximum in the first peak moves toward a larger distance, while that of the second peak moves toward a shorter distance. The first peak fully decays around 0.4–1 ps, which is faster compared to the IXS results. The rate of peak shift depends slightly on the sample temperature as shown in Fig. 2 (right). In the previous study [35] we have shown that other water models (TIP3P, TIP4P, and TIP5P) provide substantially similar results.

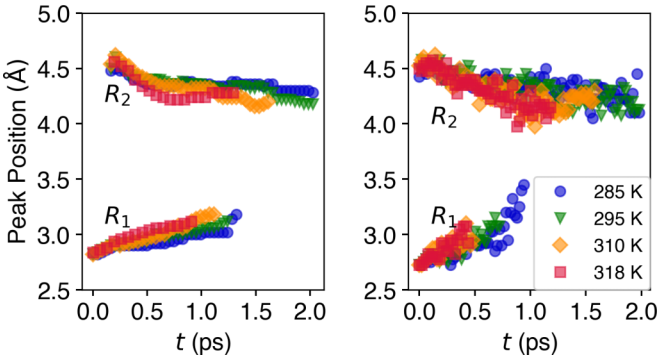

FIG. 2. Temporal changes in the first and the second peak positions, R_1 and R_2, of the Van Hove function calculated from (left) IXS data and (right) MD calculation. The temperature of the sample is shown in the inset.

B. Decay behavior of $G(R, t)$ for the first neighbors

Temporal changes in the first neighbor peak exhibit an unexpected two-step relaxation behavior. Figures 4(a) and 4(b) show the time evolution of the peak height, $G(R_1, t) - 1$, and that of the peak area, $A(t)$, for the first neighbor peak. The peak area $A(t)$ is defined as $A(t) = \int_{R_1'}^{R_1''}[G(R, t) - 1]dR$, where $G(R, t) > 1$ for $R_1' < R < R_1''$ around R_1. Two-step decay is clearly observed both in the peak height and the peak area except for the highest temperature, $T = 318$ K. The decaying behavior can be decomposed into two compressed exponential functions ($\tau_1 < \tau_2$),

$$A(t) = A_1 e^{-(t/\tau_1)^{\gamma_1}} + A_2 e^{-(t/\tau_2)^{\gamma_2}}, \tag{4}$$

with the exponents $\gamma > 1$ implying compression, while the decay at $T = 318$ K can be approximated with a single compressed exponential function. The fitting result for the peak area is shown in Table I, and values of τ_1 and τ_2 are plotted in Fig. 5. The value of γ_1 hardly varies with temperature, so we decided to fix it to that obtained for 318 K where the value of γ_1 can most reliably be determined. The decay time of the first component, τ_1, also remains unchanged with a temperature at 0.25 ps, and the value of A_1 is also insensitive to the sample temperature. However, the decay time of the second component, τ_2, varies with temperature from 0.8 to 1.1 ps.

The results of the MD simulation, shown in Fig. 6 (left), also show a two-step decay, qualitatively agreeing with the IXS results. The first decay time τ_1 is temperature independent, whereas the relaxation time of the second component, τ_2, increases with cooling. Although the temporal range of the first decay corresponds to the range where termination errors are

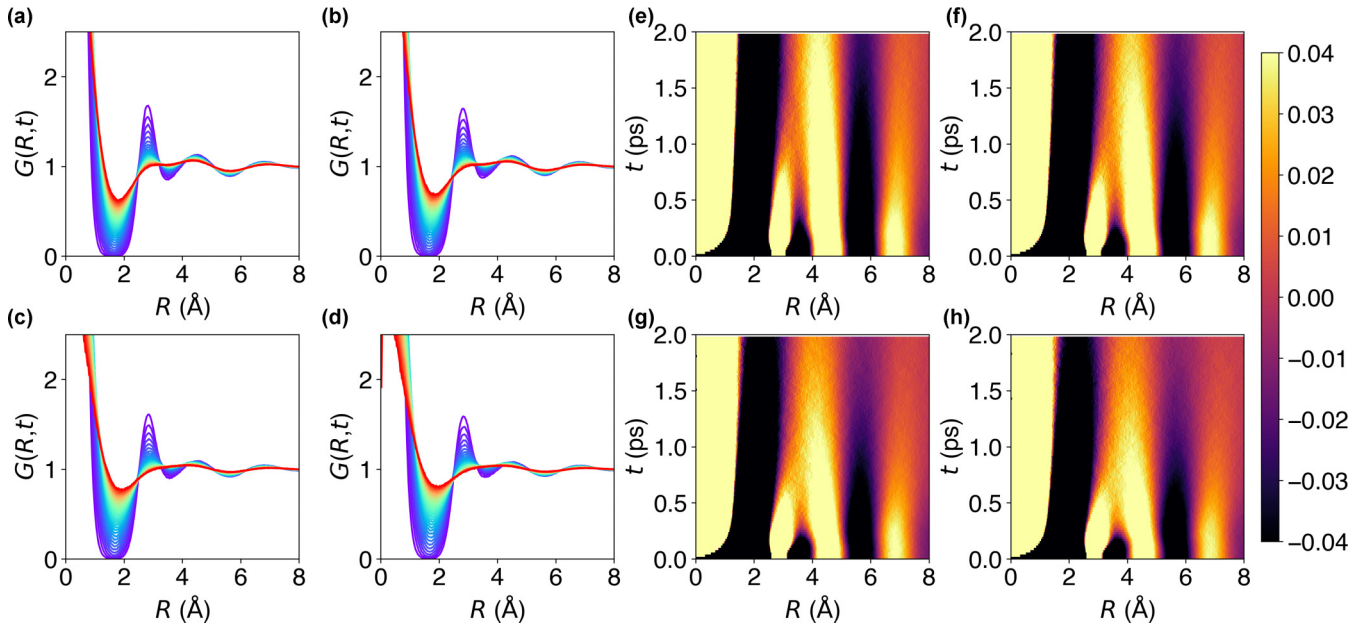

FIG. 3. The Van Hove function of water at ambient temperatures obtained from MD simulation. (a)–(d) One-dimensional profiles at 0.12 ps $< t <$ 2 ps. (e)–(h) Intensity map of $G(R, t) - 1$. Note that a narrow range is used to highlight small changes in the second and third peaks. Temperature of the water was 285 K (a),(e), 295 K (b),(f), 310 K (c),(g), and 318 K (d),(h).

significant, this agreement with the MD simulation suggests that the effects of termination errors are minimal. On the other hand, the values of the relaxation times are significantly different from the IXS results when the results of MD simulation were fitted with Eq. (4). The parameters are listed in Table II, and values of τ_1 and τ_2 are plotted in Fig. 5.

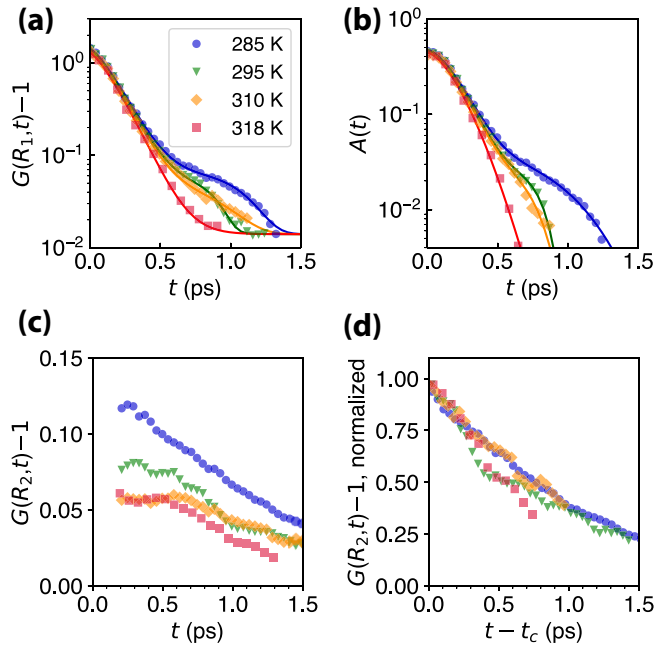

FIG. 4. Temporal changes in (a) the height of the first peak, $G(R, t) - 1$, and (b) the area of the first peak, $A(t)$, calculated from IXS results. Lines are the result of fitting using two compressed exponential functions. Temperatures are shown in the inset of the left panel. (c) Temporal change in the height of the second peak, calculated from the IXS results, and (d) its normalized intensity dependence on the reduced time.

C. Decay behavior of $G(R, t)$ for the second neighbor

Temporal changes in the peak height of the second neighbor are shown in Fig. 4(c). The peak height at $t = 0$ is higher for the lower temperature, which agrees with the previous studies of the pair distribution function of water using x-ray or neutron scattering [44]. This has been attributed to *tetrahedrality*, the degree of tetrahedral structure which is characteristic to water [12,18], and has been discussed in terms of low-density and high-density forms of water [18]. At higher temperatures (310 and 318 K), the temporal changes in the peak intensity show a plateau up to around 0.5 ps. During this time, the peak position drastically changes (Fig. 2). After the plateau, the peak intensity starts to decay with little change in the peak position. In contrast, at $T = 285$ K the peak intensity decays monotonically without a plateau. If we introduce the induction time, t_c, as the duration of the plateau and normalize the decaying behavior with the intensity at t_c, the decaying behavior of the second neighbor peak is almost temperature independent as shown in Fig. 4(d) except for small variations most probably due to experimental fluctuations. Indeed, the

TABLE I. Fitting results of the first peak area, $A(t)$, of the Van Hove function obtained by IXS.

	τ_1/ps	τ_2/ps	A_1	A_2	γ_1	γ_2
285 K	0.25	1.04	0.44	0.036	1.57[a]	3.4
295 K	0.25	0.86	0.45	0.018	1.57[a]	12.8
310 K	0.24	0.77	0.42	0.026	1.57[a]	4.1
318 K	0.25		0.45		1.57	

[a]Fixed.

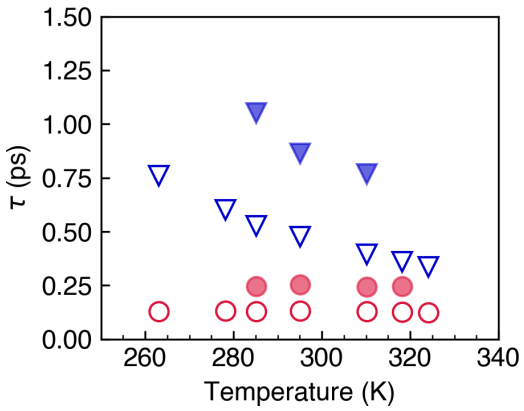

FIG. 5. Temperature dependence of τ_1 (circles) and τ_2 (triangles) obtained from IXS (closed symbols) and MD (open symbols).

MD simulation gives a similar result as shown in Fig. 6 (right). Here the normalized spectra show temperature-independent decay up to $t \sim 0.5$ ps, followed by the temperature-dependent decay, although the first plateau is not observed.

Both the IXS results and the MD results show that the dynamics for the second peak is slower than that for the first peak. This result is consistent with our prior study using simple metallic liquids; the decay time of the Van Hove function $G(R, t)$ at each peak increases linearly with R, so a higher-order peak shows a slower decay [49]. However, our current result shows not only the more gradual decay for the second peak but also much higher intensity at a later stage; the second peak remains even after the first peak entirely decays. This suggests a pronounced role of the second neighbor shell in the water dynamics.

IV. DISCUSSION

The salient features of the Van Hove function determined by IXS measurements near room temperature can be summarized as follows:

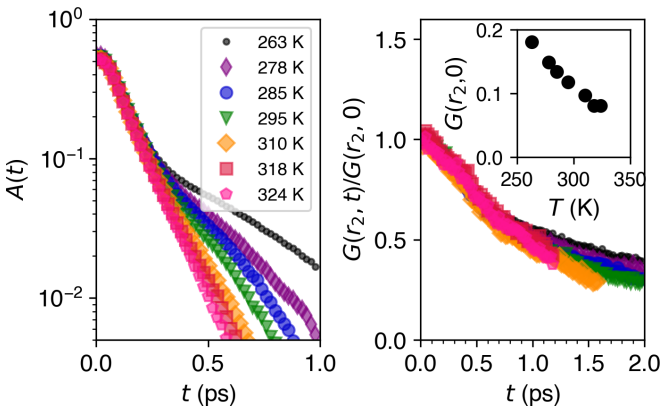

FIG. 6. Temporal changes in (left) the area of the first peak, $A(t)$, and (right) the height of the second peak, $G(R_2, t)/G(R_2, 0)$, calculated from MD simulations. The inset in the right panel shows the intensity at time $t = 0$. The temperatures are shown in the inset in the right panel.

TABLE II. Fitting results of the first peak area, $A(t)$, of the Van Hove function obtained by MD.

	τ_1/ps	τ_2/ps	A_1	A_2
263 K	0.13	0.76	0.52	0.085
278 K	0.13	0.60	0.50	0.079
285 K	0.13	0.53	0.49	0.082
295 K	0.13	0.48	0.49	0.077
310 K	0.13	0.40	0.47	0.083
318 K	0.13	0.36	0.46	0.088
324 K	0.13	0.34	0.46	0.089

The first neighbor peak shows a two-step decay: The relaxation time of the first step, $\tau_1 = 0.25$ ps, is independent of temperature whereas the second step slows down with cooling.

The intensity of the second neighbor peak shows a temperature-dependent plateau at higher temperatures, followed by a decay which is much slower than the first neighbor peak.

The first neighbor peak around $R_1 = 2.8$ Å shifts toward larger distances, while the second neighbor peak around $R_2 = 4.5$ Å shifts toward smaller distances. The movement of the second peak position is fast for $T = 310$ and 318 K up to $t = 0.5$ ps, followed by small changes around 4.25 Å, while it is monotonic for $T = 285$ and 295 K.

The shift in the second peak position corresponds to the intensity plateau.

These behaviors are not observed in a simple metallic liquid, for which a simple monotonic decay without a shift in the peak positions is observed. In the following, we discuss the possible origins of these behaviors.

A. Characteristic behaviors of water molecules

The first decay time for the first neighbor, τ_1, is temperature independent. We surmise that the first decay originates from the ballistic motions of molecules, observed for a short time (<0.3 ps) before they hit the cage of the neighbors. In solids such ballistic motions will become vibrational, but in liquids a majority of phonons are overdamped and decay before finishing one cycle [15]. The rms displacement of atoms is initially linear with time and becomes proportional to $\sqrt{t}$ just as diffusion after the cage collapses. Consequently, the initial rapid decay of the peak should be only weakly dependent on temperature, because $\sqrt{\langle v^2 \rangle} \sim \sqrt{T}$, and over a narrow temperature range it is nearly constant. Indeed, our recent simulation of a simple metallic liquid shows a similar fast initial decay and its near invariance with temperature is observed for the first neighbor peak of $G(R, t)$ [49]. This also supports our speculation that the fast decay originates from the kinetic fluctuations of molecules. The similar temperature-independent mode has been observed at 180 cm^{-1} for the vibrational dynamics with time-resolved optical Kerr effect measurement [26]. Femtosecond time-resolved infrared spectroscopy has also confirmed the existence of fast vibrational motion at around 0.17 ps, which was assigned to underdamped intermolecular coordinates of the liquid [22]. Also the intramolecular vibration may contribute the decay [50],

although the detailed contribution of intramolecular motion cannot be distinguished with our current approach using the molecular Van Hove function. These spectroscopic results require a structural model and simulations to be related to the intermolecular dynamics. Our approach using the Van Hove function enables us to observe directly the intermolecular dynamics in real space and time.

On the other hand, the second step of the decay in the first neighbor peak must correspond to the dynamics reflecting changes in the local topology of molecular connectivity. The dynamics on a similar timescale has been observed and assigned to collective structural reorganization [22], but without direct structural information. Our results show that the loss of correlation at the first nearest neighbor due to the local structural reorganization is on a picosecond timescale. The relaxation time of the second decay, τ_2, shows a slowdown with decreasing temperature and its timescale has a close relation to viscosity as discussed in the next section. As shown in Fig. 5, MD simulation underestimates τ_2 by a factor of 2. Even though the MD results are qualitatively similar to the experimental results, such quantitative differences are alarming. Incidentally, it is likely that large values of γ_2 for the measured data are merely the consequence of the energy resolution of the spectrometer which reduces the intensity at large t. This point will be investigated in the future.

An alternative interpretation of the two-step decay of the first neighboring peak is to relate it to the two-state water model which assumes a bimodal distribution of high-density liquid and low-density liquid [3,4,28]. The fact that the slower decay emerges at lower temperatures might suggest the growing population of low-density liquid upon cooling. However, our current analysis does not support nor deny the model. We have calculated $G(R, t)$ of both low-density liquid and high-density liquid to explore this scenario based on the results of MD simulation. Local structure index (LSI) [30] was used to separate each molecule into the low-density water and the high-density one. The result is shown in Fig. 7(e), which reveals that the low-density water with LSI $>$ 0.03 shows faster decay whereas the high-density water with LSI $<$ 0.03 shows slower decay at the first neighboring peak, indicating that topological changes of water molecules are slower under crowded conditions in the high-density water.

The introduction of LSI also provides a qualitative picture on the rapid peak shift at the second neighbor, which is observed for $T = 310$ and 318 K (Fig. 2). The two-dimensional maps of the Van Hove function in Fig. 7 show that the rapid peak shift is seen only for the sites with small LSI regardless of temperature and that the peak shift for the sites with large LSI is somewhat monotonic and small. This implies that the framework of tetrahedral water configurations is retained within this timescale.

It should be noted that the current simulation does not reproduce the plateau of the peak intensity observed at the second neighbor. Furthermore, the relaxation times obtained with MD are different from the IXS results. These discrepancies between the IXS results and the MD simulation may suggest that the present classical potential models do not accurately describe the local intermolecular fluctuation of water molecules nor the lifetime of a hydrogen bond because the quantum effect of water [51] on hydrogen bonds is not included in the classical

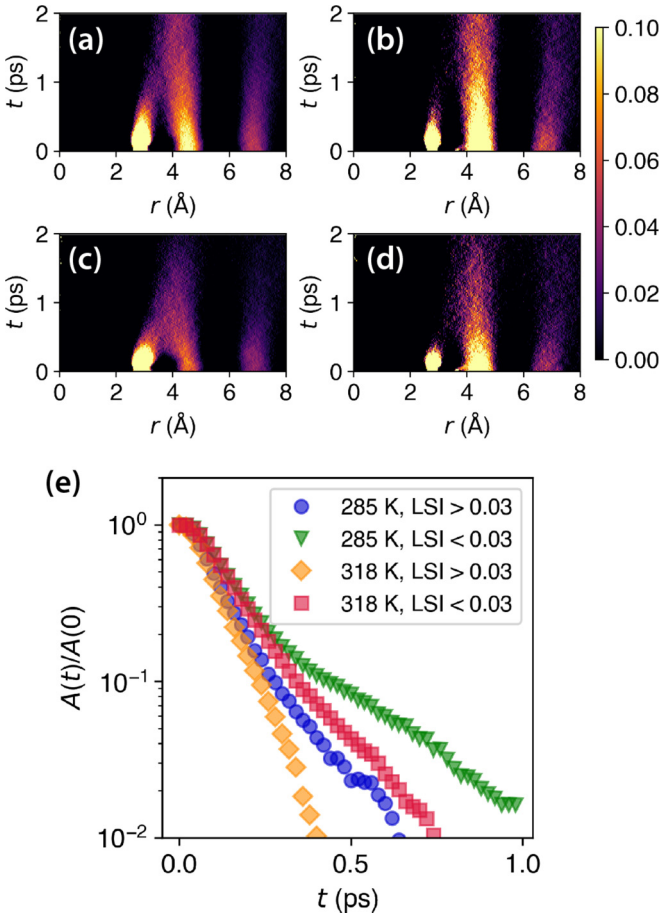

FIG. 7. (a)–(d) Two-dimensional map of calculated Van Hove functions for each LSI at 285 K (a),(b) and 318 K (c),(d). (a),(c) LSI $<$ 0.03 and (b),(d) LSI $>$ 0.03. (e) Normalized temperature evolution of the first peak intensity.

simulation model. Indeed, it is known that there are also the discrepancies between simulation and experimental results on radial distribution functions and thermodynamic properties such as density, and considerable efforts have been devoted to resolve these discrepancies. The Van Hove function analyses make it possible to directly compare the trajectory obtained by the MD simulation with the experimental results, thereby improving the water model. Quantum-mechanical calculations beyond the density functional theory, such as the path-integral quantum Monte Carlo calculation, are required to describe the dynamics of the hydrogen bond. Thus, the analysis of the Van Hove function with the classical MD using LSI or other order parameters has to be viewed with considerable trepidation.

B. Local topological rearrangement of water molecules

The peak positions of the first and second nearest neighbors evolve with time for water as seen in the two-dimensional (2D) map of $G(R, t)$ (Fig. 1), which is in sharp contrast to the case of metallic liquid [46], for which the peak positions remain unchanged. This indicates that the movements of neighboring water molecules are not random, but are highly correlated. As was discussed in the previous study, this difference can be explained by considering the local configuration of molecules

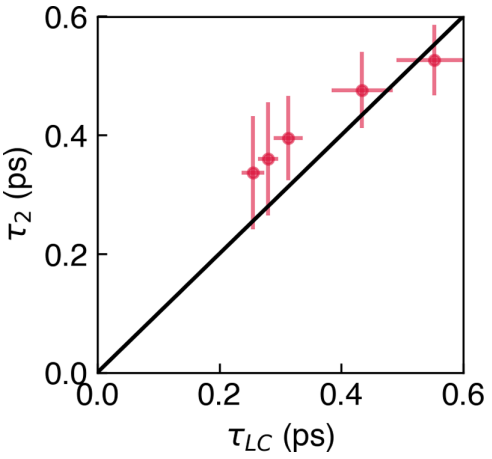

FIG. 8. The relationship between τ_2 and τ_{LC} for the calculated trajectory of water molecules using the SPC/E water model. The line shows $\tau_{LC} = \tau_2$. The error bars for τ_2 correspond to the two standard deviations of the mean. The error bars for τ_{LC} were estimated by using ten different MD runs.

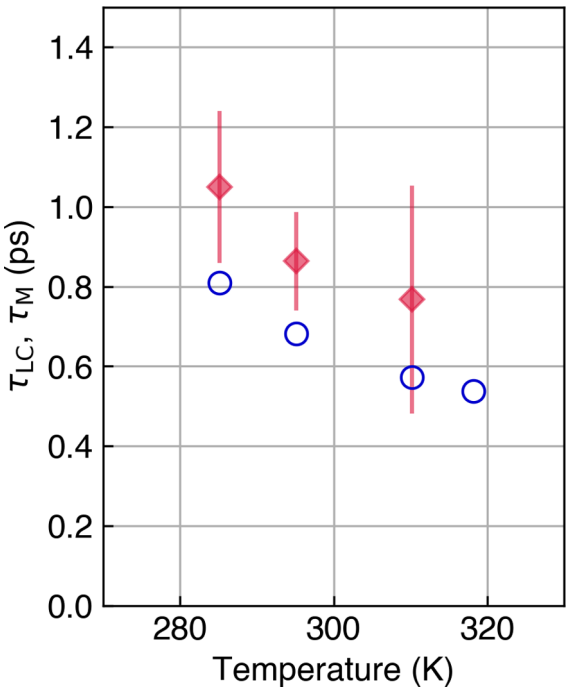

FIG. 9. Temperature dependence of the Maxwell relaxation time, τ_M (circles) and the excitation time, τ_{LC} (diamonds), derived from the IXS measurement by $\tau_{LC} \approx \tau_2$. The Maxwell relaxation time is calculated from the viscosity [54] and shear modulus, G_∞ from ultrasonic viscosity measurement [55]. The error bars for τ_{LC} correspond to the two standard deviations of the mean for τ_2.

[35]. In metallic liquids, the local coordination number (the number of nearest neighbors) is large, $N_c \sim 12$; thus bond cutting and forming are not correlated in space and time [52]. In contrast, the first and second neighbors are dynamically coupled in water due to the existence of a hydrogen bond and a small coordination number ($N_c \sim 4$). The shortening of distances between the first peak and the second peak indicates that the second neighbor water molecule moves closer to form a new hydrogen bond when a hydrogen bond between the central and the first neighbor water molecules is broken. This underscores the importance of introducing molecular connectivity and its topological rearrangement explicitly for discussing the physics of a liquid. This coupled dynamics at the first and second nearest neighbors certainly affects the decaying behavior at each neighbor, which will be addressed in the future.

C. Relationship to macroscopic properties

Here we relate the observed local dynamics to macroscopic viscosity. It is clear that exchanging the neighboring water molecules will directly influence molecular transport properties such as viscosity. To describe the local dynamics, we focus on the second decay process of the first neighbor. By inspecting the simulation results on the calculated trajectory of water molecules using the SPC/E model, we find that τ_2 is almost equal to τ_{LC}, the time for an atom or a molecule to lose or gain one neighbor [52,53]: $\tau_{LC} \approx \tau_2$ for the measured temperature range in this study (Fig. 8). In the earlier work on liquid metals, we found that τ_{LC} is equal to the Maxwell relaxation time, $\tau_M = \eta/G_\infty$, where G_∞ is instantaneous shear modulus, above the viscosity crossover temperature [52]. The same relationship has also been experimentally found in water at $T = 298$ K [35], although the estimation of τ_{LC} involved uncertainty. The current study provides more solid evidence of the equality, $\tau_{LC} \approx \tau_M$, as shown in Fig. 9, which shows the temperature dependence of τ_M and τ_{LC}. Here τ_M is calculated using the reported values of viscosity η [54] and instantaneous shear modulus G_∞ [55] and τ_{LC} is experimentally estimated by using $\tau_{LC} \approx \tau_2$. Note that τ_{LC} at $T = 318$ K is not given because we could not separate the second step decay from the first step decay in the Van Hove function at $T = 318$ K. The result shows that the microscopic timescale, τ_{LC}, is in agreement with the macroscopic timescale, τ_M. Small systematic disagreement between τ_{LC} and τ_M is within the small uncertainty with respect to the exact value of G_∞. These results support our earlier finding that the topological excitations in the atomic and/or molecular connectivity are the origin of viscosity at high temperatures [52]. The estimated value of τ_{LC} at 295 K, ~0.86 ps, is longer than the estimate in the previous study, ~0.4 ps [35]. This discrepancy originates from the much-improved statistics of the present IXS data. The high-intensity x rays from three undulators at a new IXS beamline [43] enabled us to determine the second step decay with much-improved statistics, and the configurational changes are more accurately determined.

The discrepancies between τ_{LC} and τ_M are expected to arise at temperatures lower than room temperature as is observed for metallic liquid due to the drastic slowing down induced by supercooling [52]. The upper limit of the timescale of the present result depends on the x-ray energy resolution of the measurement, whereas the energy range measured with IXS determines the lower limit. The current energy resolution is suitable for measuring the dynamics of water near room temperature but is not good enough to explore the drastic slowing down induced by supercooling. Further progress in the energy resolution or the use of an x-ray free-electron laser

for directly measuring the correlation of scattering images in the picoseconds timescale [56,57] and the use of inelastic neutron scattering with better resolution, including the spin-echo technique, would widen the timescale of the Van Hove function accessible by scattering techniques, thereby enabling the studies of atomic-scale dynamics in supercooled liquid.

V. CONCLUDING REMARKS

We report on the temperature dependence of the Van Hove function of water molecules near room temperature. Recent advances in instrumentation for inelastic x-ray scattering made it possible to measure the dynamic structure factor over a wide range of energy and momentum transfers and enabled the determination of the Van Hove function, the time-dependent atomic pair density function, by x-ray scattering experiment. Through the analysis of the Van Hove function, the timescales for the dynamic changes in local atomic configuration were determined. The results demonstrate that the time required for the local rearrangement of water molecules is directly related to the Maxwell relaxation time of the system. This corroborates the idea that the topological excitations in the atomic and/or molecular connectivity govern the viscosity of liquid. Classical interatomic potentials for water were capable of describing the local dynamics qualitatively, but there are serious discrepancies, indicating the need of fully quantum-mechanical calculations for describing the dynamics of the hydrogen bond.

ACKNOWLEDGMENTS

This work was supported by the Department of Energy, Office of Science, Basic Energy Sciences, Materials and Science and Engineering Division. The IXS experiments were conducted at BL43LXU of SPring-8 with the approval of RIKEN (Proposal No. 20170075).

[1] C. A. Angell, Insights into phases of liquid water from study of its unusual glass-forming properties, Science **319**, 582 (2008).
[2] G. N. I. Clark, C. D. Cappa, J. D. Smith, R. K. Saykally, and T. Head-Gordon, The structure of ambient water, Mol. Phys. **108**, 1415 (2010).
[3] A. Nilsson and L. G. M. Pettersson, The structural origin of anomalous properties of liquid water, Nat. Commun. **6**, 8998 (2015).
[4] P. Gallo, K. Amann-Winkel, C. A. Angell, M. A. Anisimov, F. Caupin, C. Chakravarty, E. Lascaris, T. Loerting, A. Z. Panagiotopoulos, J. Russo *et al.*, Water: a tale of two liquids, Chem. Rev. **116**, 7463 (2016).
[5] O. Mishima and H. E. Stanley, The relationship between liquid, supercooled and glassy water, Nature **396**, 329 (1998).
[6] P. H. Poole, F. Sciortino, U. Essmann, and H. E. Stanley, Phase behaviour of metastable water, Nature **360**, 324 (1992).
[7] P. Ball, Water — an enduring mystery, Nature **452**, 291 (2008).
[8] L. Pauling, *The Nature of the Chemical Bond*, 3rd ed. (Cornell University Press, Ithaca, NY, 1960).
[9] G. Hura, J. M. Sorenson, R. M. Glaeser, and T. Head-Gordon, A high-quality x-ray scattering experiment on liquid water at ambient conditions, J. Chem. Phys. **113**, 9140 (2000).
[10] C. Huang, K. T. Wikfeldt, T. Tokushima, D. Nordlund, Y. Harada, U. Bergmann, M. Niebuhr, T. M. Weiss, Y. Horikawa, M. Leetmaa, O. Takahashi, A. Lenz, L. Ojamaë, A. P. Lyubartsev, S. Shin, L. G. M. Pettersson, and A. Nilsson, The inhomogeneous structure of water at ambient conditions, Proc. Natl. Acad. Sci. USA **106**, 15214 (2009).
[11] L. B. Skinner, C. Huang, D. Schlesinger, L. G. M. Pettersson, A. Nilsson, and C. J. Benmore, Benchmark oxygen-oxygen pair-distribution function of ambient water from x-ray diffraction measurements with a wide Q-range, J. Chem. Phys. **138**, 074506 (2013).
[12] J. A. Sellberg *et al.*, Ultrafast X-ray probing of water structure below the homogeneous ice nucleation temperature, Nature **510**, 381 (2014).
[13] K. Amann-Winkel, M.-C. Bellissent-Funel, L. E. Bove, T. Loerting, A. Nilsson, A. Paciaroni, D. Schlesinger, and L. B. Skinner, X-ray and neutron scattering of water, Chem. Rev. **116**, 7570 (2016).
[14] F. Perakis, K. Amann-Winkel, F. Lehmkühler, M. Sprung, D. Mariedahl, J. A. Sellberg, H. Pathak, A. Späh, F. Cavalca, D. Schlesinger *et al.*, Diffusive dynamics during the high-to-low density transition in amorphous ice, Proc. Natl. Acad. Sci. USA **114**, 8193 (2017).
[15] F. Sette, G. Ruocco, M. Krisch, U. Bergmann, C. Masciovecchio, V. Mazzacurati, G. Signorelli, and R. Verbeni, Collective Dynamics in Water By High Energy Resolution Inelastic X-Ray Scattering, Phys. Rev. Lett. **75**, 850 (1995).
[16] G. Ruocco and F. Sette, The high-frequency dynamics of liquid water, J. Phys.: Condens. Matter **11**, R259 (1999).
[17] F. Sette, G. Ruocco, M. Krisch, C. Masciovecchio, R. Verbeni, and U. Bergmann, Transition from Normal to Fast Sound in Liquid Water, Phys. Rev. Lett. **77**, 83 (1996).
[18] A. K. Soper and M. A. Ricci, Structures of High-Density and Low-Density Water, Phys. Rev. Lett. **84**, 2881 (2000).
[19] J. Swenson, R. Bergman, and S. Longeville, A neutron spin-echo study of confined water, J. Chem. Phys. **115**, 11299 (2001).
[20] R. H. Coridan, N. W. Schmidt, G. H. Lai, R. Godawat, M. Krisch, S. Garde, P. Abbamonte, and G. C. L. Wong, Hydration Dynamics at Femtosecond Time Scales and Angstrom Length Scales from Inelastic X-Ray Scattering, Phys. Rev. Lett. **103**, 237402 (2009).
[21] A. H. Narten and H. A. Levy, Liquid water: molecular correlation functions from x-ray diffraction, J. Chem. Phys. **55**, 2263 (1971).
[22] C. J. Fecko, J. D. Eaves, J. J. Loparo, A. Tokmakoff, and P. L. Geissler, Ultrafast hydrogen-bond dynamics in the infrared spectroscopy of water, Science **301**, 1698 (2003).
[23] T. Tokushima, Y. Harada, O. Takahashi, Y. Senba, H. Ohashi, L. G. M. Pettersson, A. Nilsson, and S. Shin, High resolution x-ray emission spectroscopy of liquid water: the observation of two structural motifs, Chem. Phys. Lett. **460**, 387 (2008).
[24] J. S. Hansen, A. Kisliuk, A. P. Sokolov, and C. Gainaru, Identification of Structural Relaxation in the Dielectric Response of Water, Phys. Rev. Lett. **116**, 237601 (2016).

[25] J. D. Eaves, J. J. Loparo, C. J. Fecko, S. T. Roberts, A. Tokmakoff, and P. L. Geissler, Hydrogen bonds in liquid water are broken only fleetingly, Proc. Natl. Acad. Sci. USA **102**, 13019 (2005).
[26] A. Taschin, P. Bartolini, R. Eramo, R. Righini, and R. Torre, Evidence of two distinct local structures of water from ambient to supercooled conditions, Nat. Commun. **4**, 2401 (2013).
[27] S. Garrett-Roe, F. Perakis, F. Rao, and P. Hamm, Three-dimensional infrared spectroscopy of isotope-substituted liquid water reveals heterogeneous dynamics, J. Phys. Chem. B **115**, 6976 (2011).
[28] J. Russo and H. Tanaka, Understanding water's anomalies with locally favoured structures, Nat. Commun. **5**, 3556 (2014).
[29] F. H. Stillinger and T. A. Weber, Inherent structure in water, J. Phys. Chem. **87**, 2833 (1983).
[30] E. Shiratani and M. Sasai, Molecular scale precursor of the liquid–liquid phase transition of water, J. Chem. Phys. **108**, 3264 (1998).
[31] D. C. Elton and M. Fernández-Serra, The hydrogen-bond network of water supports propagating optical phonon-like modes, Nat. Commun. **7**, 10193 (2016).
[32] S. R. Accordino, J. A. Rodriguez Fris, F. Sciortino, and G. A. Appignanesi, Quantitative investigation of the two-state picture for water in the normal liquid and the supercooled regime, Eur. Phys. J. E **34**, 48 (2011).
[33] K. T. Wikfeldt, A. Nilsson, and L. G. M. Pettersson, Spatially inhomogeneous bimodal inherent structure of simulated liquid water, Phys. Chem. Chem. Phys. **13**, 19918 (2011).
[34] L. Van Hove, Correlations in space and time and Born approximation scattering in systems of interacting particles, Phys. Rev. **95**, 249 (1954).
[35] T. Iwashita, W. Bin, W.-R. Chen, S. Tsutsui, A. Q. R. Baron, and T. Egami, Seeing real–space dynamics of liquid water through inelastic x-ray scattering, Sci. Adv. **3**, e1603079 (2017).
[36] G. Monaco, A. Cunsolo, G. Ruocco, and F. Sette, Viscoelastic behavior of water in the terahertz-frequency range: An inelastic x-ray scattering study, Phys. Rev. E **60**, 5505 (1999).
[37] A. Cunsolo, C. N. Kodituwakku, F. Bencivenga, M. Frontzek, B. M. Leu, and A. H. Said, Transverse dynamics of water across the melting point: A parallel neutron and x-ray inelastic scattering study, Phys. Rev. B **85**, 174305 (2012).
[38] A. Q. R. Baron, in *Synchrotron Light Sources and Free-Electron Lasers*, edited by E. Jaeschke, S. Khan, J. R. Schneider, and J. B. Hastings (Springer International Publishing, Basel, 2016), pp. 1643–1719.
[39] A. Q. R. Baron, in *Synchrotron Light Sources and Free-Electron Lasers*, edited by E. Jaeschke, S. Khan, J. R. Schneider, and J. B. Hastings (Springer International Publishing, Basel, 2016), pp. 1721–1757.
[40] A. Q. R. Baron, Y. Tanaka, S. Goto, K. Takeshita, T. Matsushita, and T. Ishikawa, An x-ray scattering beamline for studying dynamics, J. Phys. Chem. Solids **61**, 461 (2000).
[41] D. Ishikawa, D. S. Ellis, H. Uchiyama, and A. Q. R. Baron, Inelastic x-ray scattering with 0.75 meV resolution at 25.7 keV using a temperature-gradient analyzer, J. Synchrotron Rad. **22**, 3 (2015).
[42] Y. Kawakita, T. Kikuchi, Y. Inamura, S. Tahara, K. Maruyama, T. Hanashima, M. Nakamura, R. Kiyanagi, Y. Yamauchi, K. Chiba, S. Ohira-Kawamura, Y. Sakaguchi, H. Shimakura, R. Takahashi, and K. Nakajima, Anomaly of structural relaxation in complex liquid metal of bismuth - Dynamic correlation function of coherent quasi-elastic neutron scattering, Physica B (to be published).
[43] A. Q. R. Baron, Status of the RIKEN NanoDynamics Beamline (BL43LXU): The Next Generation for Inelastic X-ray Scattering, SPring-8/SACLA Information **15**, 14 (2010).
[44] L. B. Skinner, C. J. Benmore, J. C. Neuefeind, and J. B. Parise, The structure of water around the compressibility minimum, J. Chem. Phys. **141**, 214507 (2014).
[45] P. J. Brown, A. G. Fox, E. N. Maslen, M. A. OKeefe, and B. T. M. Willis, in *International Tables for Crystallography*, 1st ed. (International Union of Crystallography, Chester, England, 2006), pp. 554–595.
[46] U. Dahlborg, W. Gudowgki, and M. Davidovic, Van Hove correlation functions from coherent neutron inelastic scattering, J. Phys.: Condens. Matter **1**, 6173 (1989).
[47] S. Plimpton, Fast Parakkek algorithms for short-range molecular dynamics, J. Comput. Phys. **117**, 1 (1995).
[48] M. Orsi, Comparative assesment of the ELBA coarse-grained model for water, Mol. Phys. **112**, 1566 (2014).
[49] B. Wu, T. Iwashita, and T. Egami, Atomic Dynamics in Simple Liquid: de Gennes Narrowing Revisited, Phys. Rev. Lett. **120**, 135502 (2018).
[50] G. Hinze, D. D. Brace, S. D. Gottke, and M. D. Fayer, A detailed test of mode-coupling theory on all time scales: Time domain studies of structural relaxation in a supercooled liquid, J. Chem. Phys. **113**, 3723 (2000).
[51] V. N. Novikov and A. P. Sokolov, Quantum effects in dynamics of water and other liquids of light molecules, Eur. Phys. J. E **40**, 57 (2017).
[52] T. Iwashita, D. M. Nicholson, and T. Egami, Elementary Excitations and Crossover Phenomenon in Liquids, Phys. Rev. Lett. **110**, 205504 (2013).
[53] T. Iwashita and T. Egami, Atomic Mechanism of Flow in Simple Liquids Under Shear, Phys. Rev. Lett. **108**, 196001 (2012).
[54] L. Korson, W. Drost-Hanse, and F. J. Millero, Viscosity of water at various temperatures, J. Phys. Chem. **73**, 34 (1969).
[55] W. M. Slie, A. R. Donfor, and T. A. Litovitz, Ultrasonic shear and longitudinal measurements in aqueous glycerol, J. Chem. Phys. **44**, 3712 (1966).
[56] T. Osaka, T. Hirano, Y. Sano, Y. Inubushi, S. Matsuyama, K. Tono, T. Ishikawa, K. Yamauchi, and M. Yabashi, Wavelength-tunable split-and-delay optical system for hard x-ray free-electron lasers, Opt. Express **24**, 9187 (2016).
[57] W. Roseker, H. Franz, H. Schulte-Schrepping, A. Ehnes, O. Leupold, F. Zontone, S. Lee, A. Robert, and G. Gruebel, Development of a hard x-ray delay line for x-ray photon correlation spectroscopy and jitter-free pump-probe experiments at x-ray free-electron laser sources, J. Synchrotron Radiat. **18**, 481 (2011).